Hydrodynamics and Control of Body Caudal Fin Manoeuvring

Marvin Wright, Qing Xiao, Qiang Zhu

1 Introduction

Fish have developed highly efficient swimming abilities by continuously adapting to their environmental conditions. Species of fish belonging to the category of Body Caudal Fin (BCF) generate thrust through displacement of their central lines by means of body undulation. The inherently unstable swimming states enable agile and efficient manoeuvrability through small perturbations of body kinematics[1]. Curving of the body represents a key mechanism to vector thrust in decoupled BCF swimmers and coupled Median Paired Fin (MPF) swimmers.

Body curvature enables a change of heading direction in C-starts, creating two distinct vortices from a still position to rapid acceleration[2], or during powered and unpowered turns[3]. Their high manoeuvrability enable fish to operate safely in complex environments[4], which scientists and engineers are keen to study and transfer knowledge into engineering designs. For manoeuvring, conventional Autonomous Underwater Vehicles (AUVs) usually utilise hydrofoils, reorientable propellers, or multiple propellers, which are often inefficient at low speeds and consume significant power. A fish-inspired manoeuvring method may provide a more effective alternative.
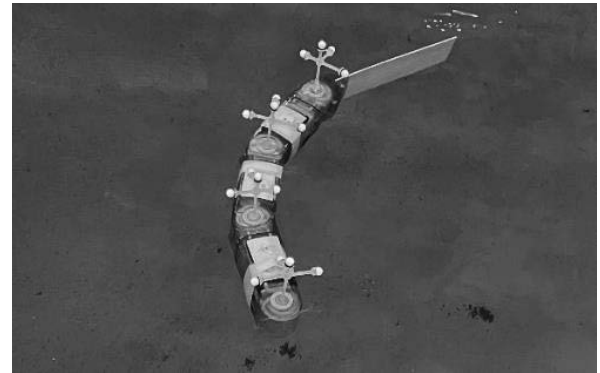
筆者紹介

Marvin Wright is a PhD candidate at the University of Strathclyde, Glasgow UK, researching bio-inspired underwater propulsion and manoeuvring. His research interests lie in experimental and numerical investigations of fluid-structure interaction and control related problems of bio-inspired underwater vehicles.

Qing Xiao is a Professor of Marine Hydrodynamics in the Department of Naval Architecture, Ocean and Marine Engineering at Strathclyde University, Glasgow, UK. She received her PhD in Fluid Mechanics from National University of Singapore. Her major research interests are computational fluid dynamics in bioinspired hydrodynamics, marine renewable energy devices and offshore fluid-structure-interaction problems.

Qiang Zhu is a Professor in the Department of Structural Engineering at the University of California, San Diego. He got his PhD in applied mechanics from the Massachusetts Institute of Technology. His research interests are in the fluid-structure interaction problems involved in ocean engineering and biomechanics.

Figure 1 Modular Magnetic Bioinspired Autonomous Vehicle (MMBAUV) performing a turning manoeuvre[5].

Indeed, existing bio-inspired designs have shown turning radii of 75 degrees per second[6], exceeding the 25-35 degrees per second of a modern enhanced torpedo shaped AUV[7].

2 Problem description

In the past, most studies of fish locomotion have been focused on steady swimming. There are only a small number of investigations into unsteady swimming, for example, the early experimental research conducted by Gray[8], the analytical work by Weihs[9], and the recent numerical work presented by Hess et al.[10].

BCF fish generate thrust through periodic displacement around their central lines to accelerate fluid along their bodies and shed vortices at their caudal fins. For an uncurved central line, the alternating vortices maintain force balance in the lateral direction over one periodic cycle so that the mean thrust is longitudinal. Through curving of the central line, the lateral symmetry is broken, leading to a change in swimming direction.
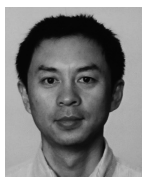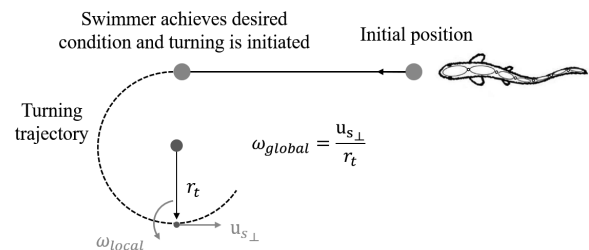

Figure 2 Simulation setup[11].

The turning moment associated with the curved centre line may result from a combination of the posterior tail fin reactive

force, the lift force acting on the anterior body and the drag force reduction by aligning with the new swimming direction.

This work focuses on the investigation of different curvature envelopes (a curvature envelope describes the curvature distribution along the centre line) and their effects on turning radius, turning velocity and power consumption. A CFD-multibody and control simulation methodology was adopted. Figure 2 shows the simulation setup of a manoeuvring BCF swimmer, starting from a still position, swimming towards a feedback-controlled state, after which the body curves according to a prescribed curvature envelope to achieve the turning manoeuvre.

3　Methodology

Numerical simulations were conducted using a fully coupled CFD-multibody algorithm with feedback control established within Ansys Fluent 22.1 and a User Defined Function. Detailed descriptions and validation of the applied methodology can be found in Wright et al.[11] and the work by Porez et al.[12], Hu[13] and Li et al.[14].

The fluid dynamics are governed by the incompressible Naiver-Stokes equations given in equations (1) and (2). In these equations $\mathbf{u} = [u, v]^T$ is the velocity, t is time, p is pressure and μ is dynamic viscosity.

$$\nabla \cdot \boldsymbol{u} = 0 \tag{1}$$

$$\frac{\partial \boldsymbol{u}}{\partial t} + (\mathbf{u} \cdot \nabla)\, \mathbf{u} = -\frac{1}{\rho}\nabla p + \frac{\mu}{\rho}\nabla^2 \mathbf{u} \tag{2}$$

Pressure-velocity coupling was applied using the non-iterative time-advancement (NITA) scheme.

Second-order pressure interpolation was applied together with the first-order implicit time marching scheme. The least square cell-based approach for the gradient and second-order upwind scheme were selected for discretisation of space.
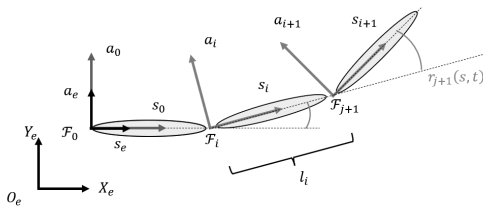

Figure 3 General multibody system setup[11].

The multi-body algorithm recursively resolves the dynamics equation. Figure 3 shows a three-body system connected by rotational joints, each with a single degree of freedom. For a continuous body, the local coordinate frame of each body is positioned on the front edge between the modules and the first frame $\mathcal{F}_0$ acts as the reference frame towards the global coordinate frame.

The joints follow actuation described by

$$r(s,t) = c_a A(s)\sin\!\left(-2\pi\big(ft + \varphi(s)\big)\right) + c_s C(s), \tag{3}$$

where $r(s,t)$ is the joint rotation angle, $s \in [0, L]$ is the Lagrangian coordinate from the swimmer's leading edge to the trailing edge, f is frequency and $A(s)$, $\varphi(s)$ and $C(s)$ describe amplitude envelope, wavelength and curvature envelope respectively. Control variables $c_a \in [0, 1]$ and $c_s \in [-0.2, 0.2]$ are updated by using a cosine transition function to avoid loss of wave shape. They are calculated through two separate PID controllers to control wave amplitude (which determines velocity) and body curvature (which determines swimming direction). Figure 4 shows the signal flow graph of the PID feedback loop.

The control error $e(t_k)$ with sampling time t_k is defined as the difference between a setpoint and the swimmer's state. By means of forward velocity and horizontal heading control, quasi-steady (QS) state is established using the difference between the swimming velocity $u_s = \sqrt{u_s^2 + v_s^2}$ and a prescribed setpoint velocity u_{set}. To maintain horizontal heading, the difference between the line-of-sight angle towards a waypoint ($P_{wp} = (20, 0)$) in the horizontal far field $\Theta_{wp} = \mathrm{atan}\left(y_{\mathcal{F}_0} - y_{wp}\big/ x_{\mathcal{F}_0} - x_{wp}\right)$ and the swimmer's heading, calculated from the coordinates of first $\mathcal{F}_0$ and second $\mathcal{F}_1$ body frame coordinates $\Theta_{swim} = \mathrm{atan}\left(y_{\mathcal{F}_0} - y_{\mathcal{F}_1}\big/ x_{\mathcal{F}_0} - x_{\mathcal{F}_1}\right)$, is minimized.
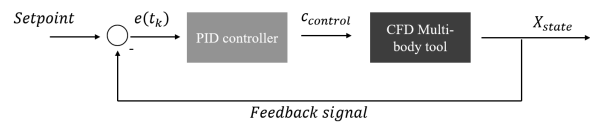

Figure 4 Coupled PID and CFD simulation signal flow graph[11].

4　Setup

The body of the swimmer is depicted as a NACA 0012 hydrofoil with chord length $L = 0.1\ m$. It is then modelled as a multi-body system consisting of 10 bodies and 9 joints, as shown in Figure 5.

The computational domain, shown in Figure 6, has the size of 25L by 8L with the swimmer initially located horizontally with the leading edge positioned 4L from the bottom boundary and 5L from the right boundary.
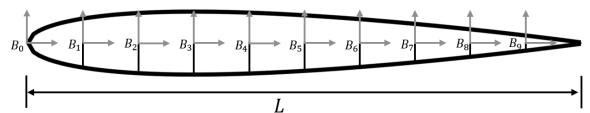

Figure 5 Simplified fish geometry modelled as multi-body NACA0012[11].

The computational domain is discretised in an unstructured mesh with edge size $\Delta_{xy} = 10/3333L$ at the swimmer's boundary and increasing to $\Delta_{xy} = 10/33L$ towards the domain boundaries. The time step is set to $\Delta t = T/250$ to satisfy the CFL criterion.

The amplitude envelope is defined following an anguilliform pattern[15] in which $A(s) = 0.125\left(s/L + 0.0315,\right)\big/1.03125$ and $\varphi(s) = 2\pi\, s/L$. A constant curvature envelope with

$C(s) = 0.15\, c_4$ and a linear curvature envelope with $C(s) = 0.15\, c_5 s/L + c_6$ are considered.

Table 1 Constant curvature envelope coefficients

κ [rad/m]	2.7	5.4	8.1	10.8	13.5
c_4	0.2	0.4	0.6	0.8	1.0

Table 2 Curvature envelope comparison coefficients

κ [rad/m]	$const$ [-]	lin_d [-]		lin_u [-]	
8.1	$c_4 = 0.6$	$c_5 = -1$	$c_6 = 1.1$	$c_5 = 1$	$c_6 = 0.1$

The parameters investigated in this study are summarised in Tables 1 and 2. The Reynolds number remains fixed at 2000.

To characterise the performance of different curvature envelopes, we propose a new performance parameter, the Cost of Manoeuvring (CoM) defined as

$$CoM = \frac{\overline{P_{in}}}{\omega_{\text{global}}} = \frac{\overline{P_{in}}}{u_{s,\perp}/r_t}. \tag{4}$$

The new parameter, analogue to the Cost of Transport (CoT), calculates the power over a velocity. However, it takes the linear and angular velocity and turning radius into account.

The average input power is calculated as the sum of cycle-averaged power at all the joints (defined as the product of cycle-averaged joint torque and angular velocity)

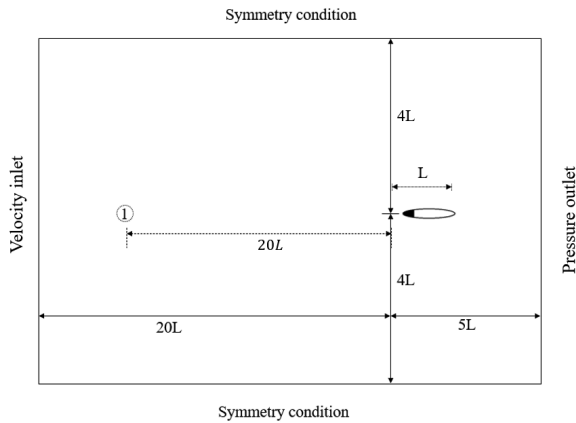$$\overline{P_{in}} = \sum_{j=1}^{9} \bar{\tau} \cdot \bar{r}. \tag{5}$$

Figure 6 CFD computational domain setup and boundary conditions[11].

5 Results & discussion

5.1 Body curvature turning mechanisms

QS state describes the condition in which the swimmer achieves cycle-averaged force equilibrium of thrust and drag forces. At this state, the cycle-averaged moment is zero and the swimmer moves in a straight line at a cycle-averaged constant velocity.

Through curvature of the central line, the equilibrium is broken and a net moment acts on the centre of mass.

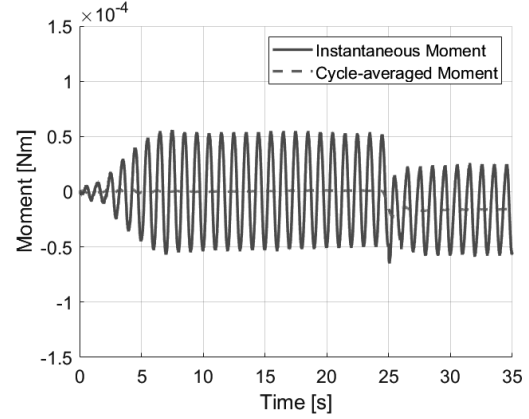As revealed in Figure 7, the swimmer experiences three

Figure 7 Instantaneous moment and cycle-averaged moment showing the three transition states[11].

phases, the QS straightline swimming state (t=25), a transition state after curving is initiated (25 < t < 27) and a QS turning state (t > 27).

Figure 8 shows the drag force and power consumption during the three phases. Notably, there is an insignificant difference in the power required for both QS states.

By increasing the curvature, the turning radius is decreased and the power consumption is increased. For the coefficients shown in Table 1, starting at κ=2.7 and $r \approx 2.8L$, the radius subsequently decreases by $\approx$ -50%, $\approx$ -66%, $\approx$ -74% and $\approx$ -79%.

The corresponding power increases from 0.179 mW by $\approx$ 3%, $\approx$ 8%, $\approx$ 13% and $\approx$ 16%.
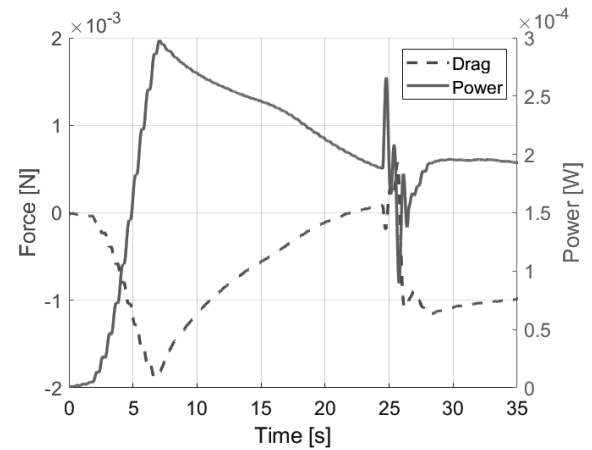

Figure 8 Cycle-averaged drag force and input power for a constant curvature envelope[11].

5.2 Curvature envelope comparison

Coefficients in Table 2 represent curvature envelopes corresponding to predominantly head curving (lin_d), tail curving (lin_u) and constant curving ($consant$) envelopes.

A comparison of the cycle-averaged drag force of the three envelopes at equal total curvature reveals two distinct phases during the transition between QS states, as highlighted in Figure 9.
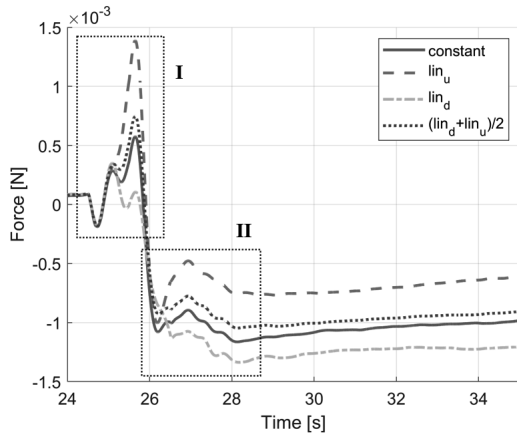
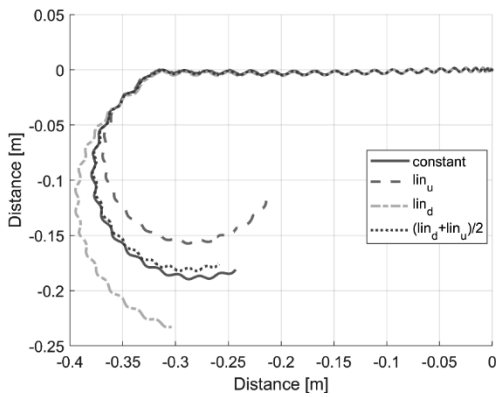Figure 9 Time histories of the cycle average drag force with different curvature envelopes[11].

Figure 10 Trajectory of a constant envelope, linear envelopes and averaged linear envelopes[11].

Phase **I** accounts for the initial drag increase of curving against the passing flow and phase **II** represents the first full curved centre line sweep. Notably, the average of the predominantly head and tail turning envelopes shows close resemblance to the constant curvature envelope.

This resemblance is also shown in the swimming trajectories (Figure 10), where it can be seen that the turning radius increases with growing head curving contribution.

Analysis of the heading angle against the passing fluid angle shows that with increasing head curvature, the heading angle lags behind the fluid angle (see Figure 11). Fish may benefit from a leading heading angle since it provides a higher turning moment.

A larger distance between the tail fin and the centre of mass may increase the moment and a strong sweep pushes the fish in front of the passing fluid. Additionally, an uncurved head may provide a dampening effect during the undulation sweep in the opposite turning direction. Figure 12 shows a schematic of these mechanisms.

The CoM results of the compared envelopes are consistent with the observations made of a smaller radius and the energetic benefit of less head curving. The CoM for predominantly head curving, tail curving and constant
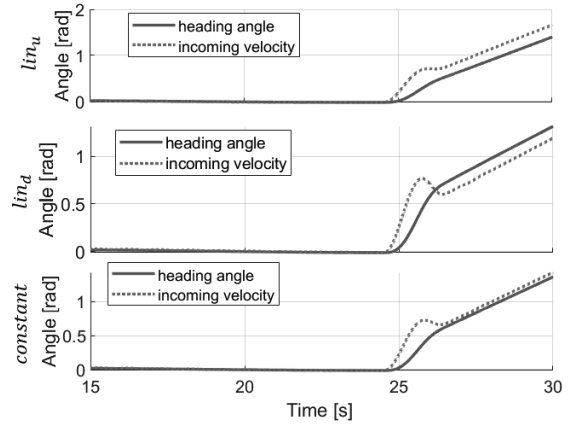

Figure 11 Instantaneous and cycle-averaged heading and incoming flow velocity angles for (a) tail turning (b) head turning (c) constant envelope[11].
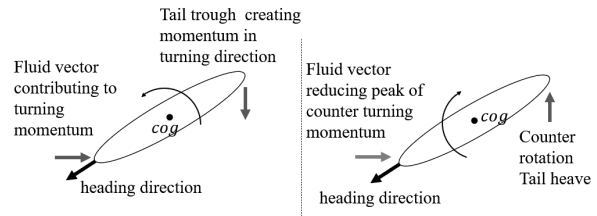

Figure 12 Schematic showing heading angle effect on moment during undulation amplitudes[11].

envelopes are 1.217 mW/rad/s, 0.7885 mW/rad/s and 0.9215 mW/rad/s respectively.

5.3 Conclusion

This work investigated the self-propelled turning performance of a two-dimensional fish with different curvature envelopes. Results show that for a constant kinematic motion envelope, the swimmer converges to a QS turning state corresponding to rectilinear swimming QS state. Further, results show the negative impact head turning has on the turning performance in terms of energetics and turning radius, which is also reflected in the newly proposed Cost of Manoeuvring parameter. Analysis of the flow field indicates that the phase difference between the swimmer and the incoming fluid as the possible reason for performance differences. In the future we plan to further validate results in lab experiments.

6 Acknowledgements

References

[1] Webb, P.W. and D. Weihs, *Stability versus maneuvering: challenges for stability during swimming by fishes*. Integrative and Comparative Biology, 2015. 55(4): p. 753-764.

[2] Epps, B.P. and A.H. Techet, *Impulse generated during unsteady maneuvering of swimming fish*. Experiments in Fluids, 2007. 43: p. 691-700.

[3] Blake, R., *On ostraciiform locomotion*. Journal of the Marine Biological Association of the United Kingdom, 1977. 57(4): p. 1047-1055.

[4] Blake, R. and K. Chan, *Models of the turning and fast-start swimming dynamics of aquatic vertebrates*. Journal of fish biology, 2006. 69(6): p. 1824-1836.

[5] Wright, M., et al., *Design and Development of Modular Magnetic Bio-Inspired Autonomous Underwater Robot – MMBAUV*. Ocean Engineering, 2023.

[6] Anderson, J.M. and N.K. Chhabra, *Maneuvering and stability performance of a robotic tuna*. Integrative and comparative biology, 2002. 42(1): p. 118-126.

[7] Randeni, S., et al., *Morpheus: An A-sized AUV with morphing fins and algorithms for agile maneuvering*. arXiv preprint arXiv:2212.11692, 2022.

[8] Gray, J., *Directional control of fish movement*. Proceedings of the Royal Society of London. Series B, Containing Papers of a Biological Character, 1933. 113(781): p. 115-125.

[9] Weihs, D., *A hydrodynamical analysis of fish turning manoeuvres*. Proceedings of the Royal Society of London. Series B. Biological Sciences, 1972. 182(1066): p. 59-72.

[10] Hess, A., X. Tan, and T. Gao, *CFD-based multi-objective controller optimization for soft robotic fish with muscle-like actuation*. Bioinspiration & biomimetics, 2020. 15(3): p. 035004.

[11] Wright, M., Q. Xiao, and Q. Zhu, *Combined hydrodynamic and control analysis on optimal kinematic parameters for bio-inspired autonomous underwater vehicle manoeuvring*. Frontiers in Physics, 2023. 11.

[12] Porez, M., F. Boyer, and A. Belkhiri. *A hybrid dynamic model for bio-inspired soft robots—Application to a flapping-wing micro air vehicle*. in *2014 IEEE International Conference on Robotics and Automation (ICRA)*. 2014. IEEE.

[13] Hu, J., *Numerical study on hydrodynamic performance of bio-mimetic locomotion*. 2016.

[14] Li, R., et al., *A multi-body dynamics based numerical modelling tool for solving aquatic biomimetic problems*. Bioinspiration & biomimetics, 2018. 13(5): p. 056001.

[15] Kern, S. and P. Koumoutsakos, *Simulations of optimized anguilliform swimming*. Journal of Experimental Biology, 2006. 209(24): p. 4841-4857.